energy&fuels

pubs.acs.org/EF
Article

Microscopic Characterization of Mineral Dissolution and Precipitation at Variable Salinity for Improved Oil Recovery in Carbonate Reservoirs

Frank Megens, Amani O. Alghamdi, Amy Z. Stetten, Mohammed B. Alotaibi, Subhash C. Ayirala, Ali A. Yousef, Igor Siretanu,* and Frieder Mugele*

Cite This: *Energy Fuels* 2024, 38, 6723−6737

ABSTRACT: Aging of carbonate mineral surfaces in brines of variable salinity and crude oil leads to massive transformations of surface topography and chemical composition including the formation of mixed organic−inorganic interfacial layers. The response of these interfacial layers to variations in brine composition is responsible for local (chemical) wettability alteration and therefore becomes the main microscopic driver for improved oil recovery in low-salinity water flooding or SmartWater flooding. In this study, a new method was developed to directly visualize local nanoscale dissolution and (re)precipitation around the three-phase contact line on model calcite surfaces in the presence of crude oil and ambient brine upon aging. The sessile microscopic oil drops on calcite surfaces were exposed to brines of variable composition at room temperature (22 °C) and at elevated temperatures (95 °C) for up to 2 weeks. Brines ranged from hypersaline formation water to diluted high-salinity water, in part enriched with Mg^{2+} or SO_4^{2-} ions. In situ optical and ex situ atomic force microscopy (AFM) imaging of the calcite surfaces was performed prior to and after aging, complemented by confocal Raman imaging. Optical images show that crude oil drops remained attached to the mineral surfaces throughout all aging procedures studied and displayed only occasional minor relaxations of their shape at elevated temperatures. Ex situ AFM images after calcite cleaning and drying displayed strong marks of the original droplet positions that appeared either as holes or as protruding mesas with respect to the surrounding surface level, with height differences up to several hundred nanometers. The sessile oil drops are thus found to protect the underlying calcite surface from both precipitation and dissolution, in overall agreement with the macroscopic calcite saturation of the brines. The qualitative trends are consistent for all conditions investigated, notwithstanding a higher degree of variability at elevated temperatures and upon preaging in oil-equilibrated formation water. In contrast to the calcite−brine interface that undergoes these massive transformations, the oil−calcite interface remains overall remarkably inert. Only at 95 °C does the occasional appearance of roundish rims accompanied by hillocks suggest the growth of water drops during aging, possibly via exchange across thin aqueous layers.

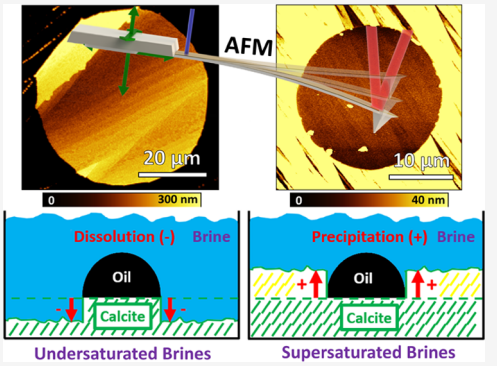

1. INTRODUCTION

Substantial efforts are devoted to improving our understanding of the processes that govern the efficiency of the displacement of crude oil by injecting brines of controlled composition. In particular, the improvement of the recovery factor by reducing the salinity of the brine and/or by adding selected "smart" ions has attracted considerable attention in recent years.[1−8] While a reasonable consensus regarding the underlying mechanism has emerged in the case of sandstone reservoirs, the principles controlling the success of low-salinity water flooding (LSWF) in carbonate reservoirs have remained controversial.[9] One of the challenges in solving the problem is that there are most likely several mechanisms at play that conspire to alter wettability in different ways, depending on the specific crude oil−brine−rock (COBR) system under investigation. A second challenge is that conclusions regarding the underlying molecular mechanisms are often inferred from macroscopic observations, such as effluent analysis in core flood experiments, without actual detailed microscopic characterization. While progress in, e.g., X-ray tomographic imaging has revealed impressive new insights regarding the distribution of oil and brine on the pore scale in recent years, the truly microscopic, i.e., molecular scale processes, that control variations of the oil−mineral adhesion and wettability still remain below the resolution limit of state-of-the-art instruments and therefore still require indirect inferences.[10]

Received: November 13, 2023
Revised: March 20, 2024
Accepted: March 21, 2024
Published: April 4, 2024

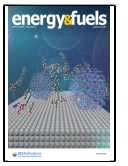

https://doi.org/10.1021/acs.energyfuels.3c04467
Energy Fuels 2024, 38, 6723−6737

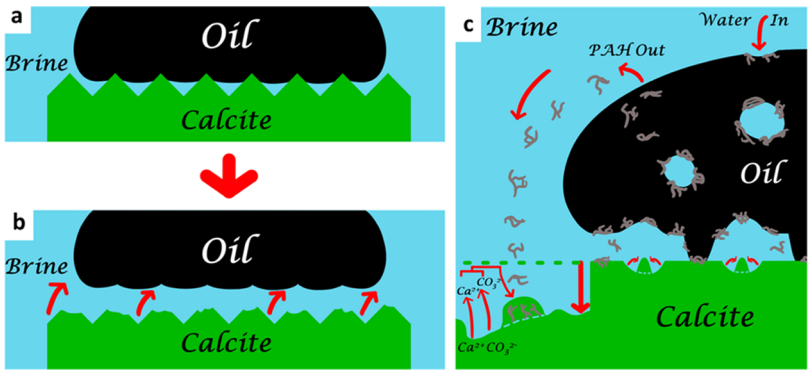

Figure 1. (a, b) Schematic representation of how mineral dissolution could cause oil release. (c) Schematic representation of the oil–brine–mineral system, showing several potential processes occurring at all three types of interfaces (oil–brine, oil–mineral, and brine–mineral).

Throughout this work, we will use the term "wettability" in its physicochemical sense equivalent to a local contact angle. This is simpler and more fundamental than the complex oil retention indices that are often used in petroleum engineering to describe the "wettability" of a porous medium. Herein, the used term "wettability" thus excludes any effect of pore geometry and history-dependent oil and brine distributions that are important for the overall recovery but act only on larger scales than the primary chemical processes of interest in this work. Atomic force microscopy (AFM) provides sufficient resolution and has revealed exquisite details on the structure, hydration, and ion adsorption at mineral–electrolyte interfaces.[11−15] Also, recently, Savulescu et al.[16] used in situ AFM to visualize in 3D the *n*-decane droplets on a calcite in seawater, the calcite surface underneath, and the effect of nanoscale surface features on the drop shape and contact angle distribution. Yet, being a delicate surface technique and being difficult to apply in complex multiphase environments, insights from AFM have largely been limited to idealized model systems.[16−19]

To understand the processes involved in the recovery process, it is useful to recall that crude oil, brine, and rock have typically been in contact for millions of years before the exploitation of an oil reservoir is initiated. Throughout this time, the COBR system has evolved toward a form of equilibrium state, in which oil and water and all solutes have partitioned in the bulk according to the respective solubilities in the fluid phases. Solutes are adsorbed at the solid–liquid and liquid–liquid interfaces. Since crude oil contains a huge number of interfacially active species, this results in adsorption layers of typically rather complex composition and mechanical properties.[20−22] Depending on their reactivity, minerals also participate in this equilibration process by dissolving, reprecipitating, and possibly recrystallizing into more stable species. This is particularly important for carbonate minerals, where these processes lead to the formation of composite films during diagenesis that incorporate organic material originating from the crude oil as well as reprecipitated and recrystallized carbonate minerals.[22−25] Chen et al. reproduced these conditions by aging calcite samples in formation water that had been pre-equilibrated with CRO.[26,27] This leads to the formation of organo-ionic layers at the solid–liquid interface with a thickness of a few tens of nanometers. More recently, Rao et al. presented an even more extended analysis of the formation and composition of such interfacial layers upon subjecting freshly cleaved calcite surfaces to a variety of aging protocols.[22,28−30] Surface restructuring and the formation of mixed organic–inorganic compounds were shown to be particularly pronounced upon aging the surfaces in CRO. These complex interfacial layers rather than a bare calcite surface should therefore be considered as the "relevant reactive surface" for improved oil recovery (IOR) processes.

For the oil–brine interface, information about interfacial layers can be obtained by using interfacial rheology. Such studies revealed that the interfacial layers can be very responsive to variations of the ambient temperature and brine compositions and can display relaxation times of several days.[22,25,31−35] Owing to the irreversibility of the adsorption process and their "independent life", these interfacial layers have also been denoted as "interphases".[36] Compared with the oil–brine interface, the interfacial layers adsorbed to the solid–liquid interfaces are more difficult to access for in situ characterization tools. In contrast to the liquid–liquid interface, the solid surface offers binding sites where polar or charged organic molecules anchor to the substrate. Molecule–substrate bonds can be mediated by ions, in particular multivalent ones, as in the multiple-ion-exchange (MIE) model of low-salinity water flooding,[37−39] and they can involve hydration water. Yet, notwithstanding these differences in interfacial affinities, there is little reason to believe that soft viscoelastic layers of adsorbed polar organic molecules should not form in a very similar manner at the mineral–oil interface, as already pointed out in the late 1990s.[40,41] Hence, it is plausible that interphases at the solid–liquid interface should be similarly responsive to external stimuli, such as variations of the salinity and composition of the brine. Chen et al.[26,27] found that the interphases display poor adhesion to the underlying calcite substrate and delaminate in the form of "flakes" in low-salinity brine. An AFM study by Kumar et al.[42] reported a similar "patchy" structure of the surface after exposure to low-salinity brines, yet without referring explicitly to flakes. However, those authors demonstrated that the organic layers deposited upon aging in crude oil (CRO) at elevated temperatures swell and soften upon exposure to brines of decreasing salinity. This process has been attributed to an osmotically driven absorption of water into the organic layer. Along the same lines, Rao et al. observed in nonlinear sum frequency generation (SFG) spectroscopy measurements an enhanced response and reorganization of polar and nonpolar groups in an organic layer adsorbed to a calcite interface upon reducing brine salinity.[22] The response of these layers has an important impact on the adhesion of crude oil to the mineral surface and thus on the wettability of the system, as also reported by Chen et al.[26,27] Mohammadi et al.[25] also reported

https://doi.org/10.1021/acs.energyfuels.3c04467
Energy Fuels 2024, 38, 6723−6737

Table 1. Brine Compositions

brine composition (mmol/L)	FW (formation brine)	HSW (high-salinity water)	10× dil. HSW	4× [SO_4^{2-}], 10× dil. HSW	4× [Mg^{2+}], 10× dil. HSW
NaCl	2590	796	79.6	75.6	1.52
$CaCl_2{\cdot}2H_2O$	476	16.2	1.62	1.62	1.62
$MgCl_2{\cdot}6H_2O$	100	86.8	8.68	8.68	34.7
$MgSO_4{\cdot}7H_2O$	3.62	4.4	0.44	0.44	0.44
$NaHCO_3$	5.80	1.97	0.197	0.197	0.197
$NaSO_4$	0	0	0	1.33	0
pH	6.5	7.8	7.4	7.4	7.4
pH Minteq (22 °C/95 °C)	8.35/8.31	8.18/8.11	7.37/7.55	7.38/7.55	7.35/7.21
pH (sample aging 2w, RT)	6.66	7.83	7.82 7.67	7.68	7.75
pH (sample aging 1w, 95 °C)	6.48	7.5	7.6	7.5	7.54
ionic strength (mol/L)	4.34	1.13	0.113	0.113	0.113
total dissolved solids (ppm)	214496	57304	5730	5686	3644
saturation index (SI) w.r.t. calcite at RT	0.805	0.443	−1.631	−1.639	−1.643
saturation index (SI) w.r.t. calcite at 95 °C	1.627	1.24	−0.792	−0.802	−0.833

that once the low salinity invades a porous system etched directly on a calcite crystal, the response of interfacial layers and wettability alteration is noninstantaneous, and the rate of oil recovery is very slow (over a time scale of days to several weeks), with oil being removed or "peel-off" layer-by-layer.

Improvements in oil recovery upon reducing brine salinity due to wettability alteration therefore involve the response of the complex interphases at all three types of interfaces (i.e., oil−brine, oil−mineral, brine−mineral) involved. While generally accepted as a significant factor behind LSWF effectiveness,[9,43−48] the chemical mechanism behind wettability alteration in sandstones and carbonates need not be the same.[49] The reactivity of minerals in carbonate reservoirs furthermore introduces extra complexity compared to inert sandstone reservoirs, giving rise to additional chemical mechanisms that may impact oil wettability. It is well established, e.g., by chemical analysis of the elute from core flood experiments that LSWF with carbonates is usually accompanied by mineral dissolution and ionic exchange at the surface.[50−53] To what extent this contributes to the IOR, however, is still under debate. Figure 1a shows a picture originally proposed by Hiorth et al.[54] that is frequently invoked to rationalize mineral dissolution-induced oil mobility in carbonates. According to this scenario, the oil initially adheres only to the top of the rough mineral surfaces (Figure 1a). These anchor points get eroded away as the mineral dissolves in the presence of undersaturated brine (Figure 1b). Gutters and wedges underneath the oil drop may play an important role in admitting diluted brine to the contact spots to initiate dissolution. In the case of less rough surfaces, molecularly thin aqueous wetting films may carry the transport of ions, albeit presumably in a less efficient manner. Clearly, this simplistic picture—if at all applicable—should be extended to include the presence of the various responsive interfacial layers, as illustrated in Figure 1b.

While frequently cited, to the best of our knowledge, the microscopic aspects of mineral dissolution and their dependence on brine composition in IOR have never been scrutinized in detail. Instead, most arguments are based on macroscopic observations in combination with more or less simplistic models that do not provide justice to the complexity of the interfaces and interphases involved. Even a pure calcite crystal in contact with brine displays a rather complex behavior, in particular at elevated temperatures.[55,56] The calcite−brine interface is characterized by continuous dissolution and reprecipitation involving various crystalline and amorphous phases of $CaCO_3$. As a consequence, surface morphologies evolve continuously, e.g., as initially hydrous amorphous nuclei precipitate and subsequently recrystallize into one of the anhydrous crystalline polymorphs.[57−60] Frequently, it is believed that these processes follow a nonclassical nucleation path, with phase separated prenucleation clusters forming in the fluid phase. Despite it being known that both inorganic (ionic) and organic (protein) components can influence the stability of these amorphous phases,[61−64] the obviously very subtle balance of both equilibria and kinetic pathways is in general not well understood. This is illustrated, for instance, by the ability of biological organisms such as coccoliths to control the growth of solid carbonate phases into the most elegant shapes by secreting minute amounts of suitable proteins.[65−68] Clearly, water-soluble components of crude oil should be expected to affect the dissolution, precipitation, and crystallization $CaCO_3$ in a similar, albeit less beautifully controlled-manner. Indeed, recent experiments involving Atomic Force Microscopy (AFM) and confocal Raman microscopy (CRM) imaging demonstrated dramatic differences in surface topography and chemical composition upon extended aging freshly cleaved calcite surfaces in brines that were or were not pre-equilibrated with crude oil.[28,29] In a different experiment, the presence of acidic organics in the brine that can form organo-metallic complexes and thereby scavenge Ca^{2+} ions was shown to dramatically enhance calcite dissolution.[69] A proper assessment of the microscopic mechanism of mineral dissolution in oil recovery therefore requires detailed experiments involving suitable aging protocols that involve both brines and crude oil and allow for nanoscale characterization of the resulting surfaces.

To gain insights into the microscopic mechanism and consequences of mineral dissolution in carbonate reservoirs, we developed a protocol to deposit CRO drops with diameters of a few tens of micrometers onto calcite substrates and age them for up to 2 weeks in brines of variable composition at room temperature (RT) and at elevated temperature (95 °C). After completion of the aging steps residual oil was removed, and the samples were cleaned for subsequent topographic imaging by AFM and chemical characterization by CRM. The key result is that the oil drops act like masks that protect the calcite substrate from the influence of the ambient brine: for

https://doi.org/10.1021/acs.energyfuels.3c04467
Energy Fuels 2024, 38, 6723−6737

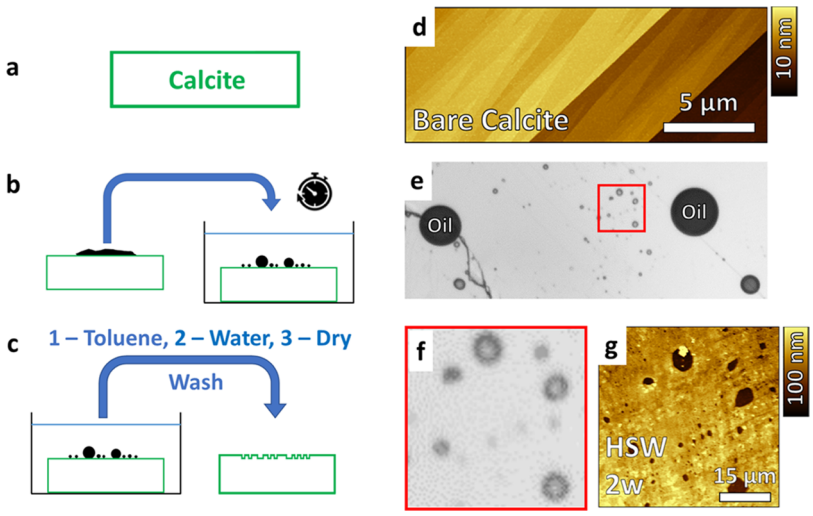

Figure 2. (a–c) Schematic representation of the experimental aging process of oil-covered calcite in brines at RT, starting from freshly cleaved calcite (a), to oil deposition and aging over time in brine (b), and to washing and drying of the samples after aging (c). (d) AFM topography scan of freshly cleaved calcite. (e) Optical photo of oil droplets on calcite while submerged in brine. (f) Zoomed-in optical photo of several oil droplets in close proximity, corresponding to the highlighted red box in (e). (g) AFM topography scan of calcite sample after aging and washing procedures, at the location corresponding to the sample area shown in (f).

undersaturated brines, the substrate dissolves next to the oil drops leading behind a mesa-like plateau of calcite in the end. For supersaturated brines, $CaCO_3$ precipitation around the drop leaves behind circular holes in the substrate with a depth corresponding to the thickness of the additionally precipitated material. In both cases, drops remain pinned at their original locations and do not become mobilized. Qualitatively similar trends were observed both at RT and at 95 °C and upon addition of specific potential determining ions (Mg^{2+}, SO_4^{2-}). In particular, at high temperatures, statistical variations were more pronounced; variations in topography and Raman spectra indicate an overall enhanced turnover of material in dissolution and precipitation.

2. METHODS AND MATERIALS

2.1. Materials. Mineral samples used in the experiments were Iceland spar calcite (Ward's Science), which were freshly cleaved into small ≈1 cm^2 pieces before use. Crude Oil (CRO) samples were obtained from a carbonate reservoir. Five different types of brines were prepared by dissolving reagent-grade chemicals (Sigma-Aldrich) in deionized water (18.2 MΩ·cm Milli-Q). The salt content and compositions of these brines are specified in Table 1. The brine suspensions were stirred overnight and filtered over a 0.2 μm PES (poly(ether sulfone)) filter before use. Aging of the oil–brine–calcite system at RT was performed in polystyrene 6-well plates using 8 mL of brine for each well. Any aging at 95 °C was done in an oven using a tightly sealed aluminum six-well plate, each well lined with either a glass or PTFE (poly(tetrafluoroethane); Teflon) Petri dish (holding around 6 mL of brine) to avoid interactions between the metal and brine. Unless specified otherwise, measurements in this work were conducted at the RT.

Formation water (FW) mimics a brine of very high salinity as typically encountered in natural carbonate reservoirs. High-salinity water (HSW) has a composition similar to that of the regular injection water. 10× dil. HSW and its SO_4^{2-}- and Mg^{2+}-enriched variants are low-salinity brines commonly considered for improved oil recovery (IOR). Saturation Indices $\left(SI = \log\left(\frac{IAP}{K_{sp}}\right)\right)$ were computed using Visual MINTEQ (Table 1). As indicated by the negative sign of the SI, the three diluted brines are undersaturated with respect to calcite; in contrast, FW and HSW are both supersaturated (Table 1). As expected, based on the inverse solubility of calcite with respect to temperature, all brines become nominally more saturated at 95 °C compared to RT. Note that the Saturation Index values reported are based on the Davies approximation for the activity coefficients, which is not quantitatively accurate at high salinities such as FW and HSW. Other solid calcium carbonate polymorphs are less stable for the thermodynamic conditions under consideration; yet, possible mixed organo-inorganic phases are not considered. Notwithstanding these limitations, we expect the qualitative trend toward higher supersaturation at elevated temperature to prevail.[70]

The used oil is a "dead" crude oil (CRO) sample obtained from a carbonate reservoir. The physicochemical characterization of CRO was performed by a certified laboratory at Saybolt Nederland B.V., and viscosity was measured with a Haake RS600 controlled stress rheometer using a Couette geometry and reported in our previous works.[22,28,71,72] The results of the CRO compositional analysis are shown in the Supporting Information, Table S1. The CRO was stored in airtight containers and agitated before use to promote the homogeneous distribution of components. The CRO was used without dilution or filtering.

2.2. Equilibration of Formation Brine (FW) and Crude Oil (CRO). Four small pieces of Iceland spar calcite were added to a 500 mL glass bottle, before filling it with equal parts (125 mL each) of FW and CRO. After degassing in a desiccator (20 min), the fluids were equilibrated for 48 h at 95 °C. Three times per day, the mixture was gently shaken to refresh the oil/brine interface. During the equilibration, polar organic material is transferred from the crude oil to the formation brine. Earlier UV/vis absorption measurements showed that the amount of transferred organic material corresponds to an equivalent of approximately 31 mg/L (aromatic) humic acid.[28] After cooling to room temperature, the equilibrated oil (eqCRO) and brine (eqFW) phases were separated using a separation funnel, capturing the fractions in individual glass bottles (250 mL).

2.3. Calcite Sample Preaging. Unless noted otherwise, CRO droplets were deposited directly onto freshly cleaved calcite surfaces. Occasionally, calcite samples were preaged in eqFW for comparison in a small glass bottle for 16 h at 95 °C. During the aging, the variation in pH of brines is less than ≈0.3 units (Table 1). Subsequently, they were briefly rinsed with deionized water (18.2 MΩ·cm Milli-Q) and dried under nitrogen to remove any salt deposited by brine evaporation during preaging. Such preaged samples display a layer of reprecipitated nanoparticles consisting largely of calcite with some incorporated Mg and aromatic organic material.[22,28]

https://doi.org/10.1021/acs.energyfuels.3c04467
Energy Fuels 2024, 38, 6723–6737

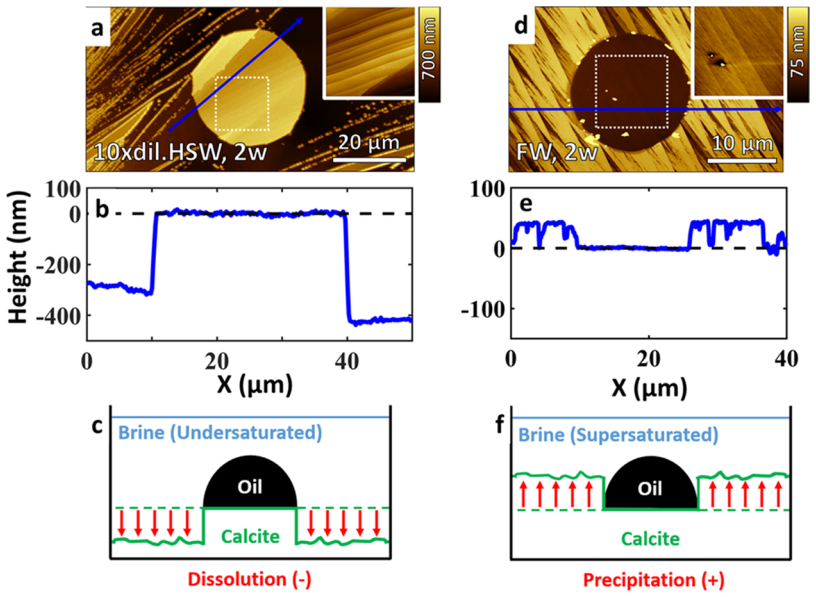

Figure 3. AFM topography scans of oil droplet locations on calcite after aging for 2 weeks at RT in (a) 10× dil. HSW and (d) FW, with an inset showing the corresponding detailed views of the oil−calcite contact areas. Height profiles corresponding to the blue arrows in (a) and (d) are shown in (b) and (e), respectively, shown at different scales. Schematic overviews of the system during aging in 10× dil. HSW and FW are given in (c) and (f), respectively.

2.4. Amplitude Modulation Atomic Force Microscopy (AM-AFM). Dynamic amplitude modulation atomic force microscopy (AM-AFM) imaging in air was used to obtain surface topographical height maps of the substrate, using a Bruker Dimension ICON instrument and NSC-36 probes (MikroMasch, tip radius r < 20 nm, cantilever spring constant k = 0.6−2 N/m). Scans were recorded in the air at a resolution of 512 × 512 pixels at a 1:1 X/Y ratio, at scan rates between 0.2 and 0.7 Hz. Data processing and exporting of the images were performed using the software package Gwyddion.[73] To protect tip sharpness and the sample, i.e., to minimize the force applied on the sample, the amplitude signal was not allowed to drop below 85% of its free oscillation amplitude. Prior to use, AFM tips were cleaned by rinsing with isopropanol, ethanol, and water and exposed to oxygen plasma (PDC-32G-2, Harrick Plasma) for 15−30 min.

3. RESULTS

3.1. Development of Sample Preparation Procedure. The first step of our experiments is to develop a procedure that allows us to analyze the response of partly oil-covered calcite surfaces to variable brine compositions upon aging at different temperatures. We start with a freshly cleaved calcite sample (Figure 2a). AFM topography images of the surface display steps of variable height up to several nanometers on the (10.4) cleavage plane (Figure 2d). The steps on the cleavage plains typically form sharp triangular structures with narrow opening angles.

Next, a small amount (2 μL) of crude oil was deposited onto the surface in ambient air. The oil spontaneously spreads into a puddle with a diameter of several millimeters. Within a few seconds, the samples are immersed in the brine of interest. The oil puddle immediately begins to recede (Figure 2b) and breaks up into droplets with a widely variable size from a few micrometers up to occasionally more than 100 μm (Figure 2b,e). The system thus contains calcite in contact with both oil and brine, as is commonly encountered in actual reservoirs. We emphasize that the initial CRO deposition in air implies an initially direct CRO−mineral contact without any intervening brine layer. This was found to be essential for the reproducibility of the preparation process. Along the edge of the oil drops, true three-phase contact lines (oil−brine−mineral) are thus formed. The samples were then left to age for up to 2 weeks in the brine in separate, closed containers at room temperature (22 °C) for the majority of the samples in this study. To explore the effect of the aging temperature, a few samples were aged at 95 °C.

Optical images taken before and after aging show that the oil drops typically neither move nor detach from the surface during aging (Figures S1 and 2e). This indicates that the contact lines remained pinned throughout the aging process. Images taken from the side further confirm the pinning, as contact angles do not change during aging (Figure S2) at RT in low-salinity 10× dil. HSW over a period of 90 h. This behavior (i.e., oil drops typically neither move nor detach) was consistently observed independent of brine composition and aging time, although for similar system materials (crude oil and calcite) and fluid compositions earlier studies[22,26−28] reported changes in macroscopic scale, i.e., more water-wet contact angle of eqCRO droplets on calcite substrates in the low-salinity brines. Yet, perhaps this is not surprising considering macroscopic contact angle measurements suffer from the fact that the systems are usually not in mechanical equilibrium because contact angle hysteresis is commonly high and contact lines are pinned to local surface defects (as observed here).

Afterward, most of the oil is removed from the drops using a pipet and the samples are taken out of the brine (Figure 2c). To remove the small residues of excess oil at the locations of the original drops, the samples are washed with a gentle stream of toluene (10 mL). Subsequently, the sample is immersed in Milli-Q water for 10 s to remove any residual salt. Finally, the samples are dried with a nitrogen stream and stored in a nitrogen compartment until further characterization.

3.2. Variation of Surface Morphology upon Aging. AFM imaging of the surfaces reveals easily distinguishable circular features exactly at the locations that were previously covered by oil drops during aging (Figure 2g). Interestingly,

https://doi.org/10.1021/acs.energyfuels.3c04467
Energy Fuels 2024, 38, 6723−6737

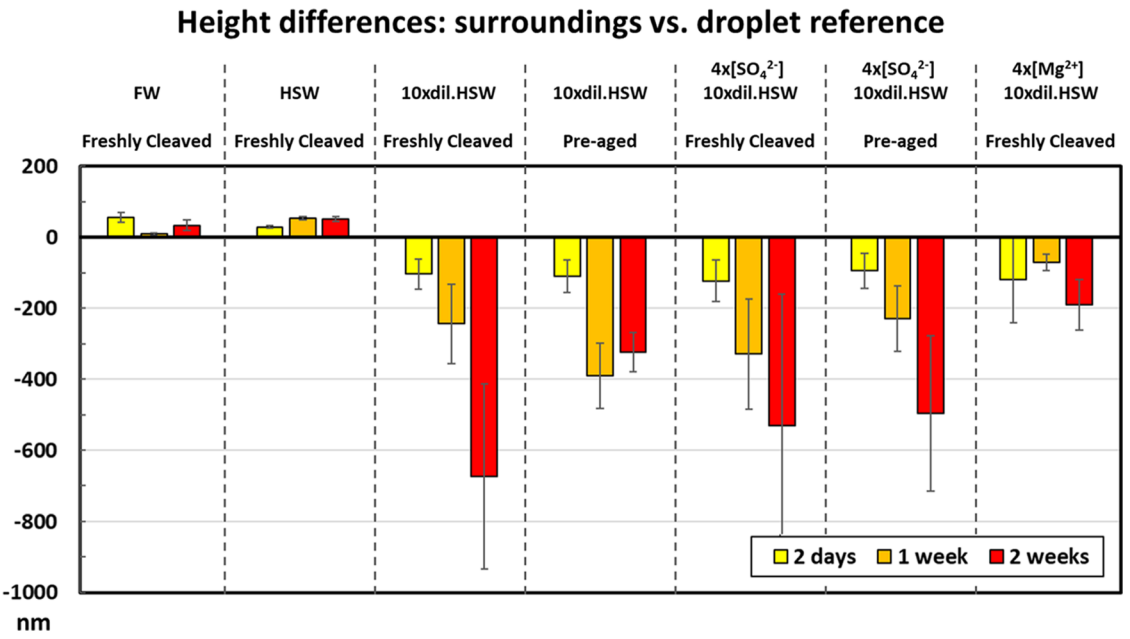

Figure 4. Height differences between droplet locations and their surroundings as extracted from AFM high profiles, after oil droplet-covered calcite was aged at RT in all of the brines listed in Table 1. Calcite was either freshly cleaved or preaged in eqFW. Error bars represent statistical errors based on 5−20 droplets per condition.

these footprints can be either lower or higher than the surrounding level of the surface (Figure 3), i.e., they appear either as holes or as mesa-like protrusions with depths (or heights) ranging from a few tens to several hundreds of nanometers (Figure 3).

For 10× dil. HSW aging brine, the oil footprint forms a plateau (Figure 3a), whereas for FW aging brine, it forms a hole (Figure 3d). Zoomed views of the bottom of the holes and the top of the mesas typically appear to be very similar to the original calcite surface prior to aging (Figure 2d). In contrast, the morphology of the surrounding area is clearly changed and rougher than before. For dilute aging brines, the surrounding of the mesas often displays many small deposits, or "bumps", that decorate the steps on the surface and form continuous chains (Figure 3a). Experiments for various fluid compositions display a clear correlation between the appearance of the holes or mesas and the composition of the aging brine, i.e., undersaturated brines lead to mesa-like protrusions and supersaturated brines lead to holes (see Figure 4 and Table 1).

Combining all of these observations, we arrive at the following picture: the calcite surface massively transforms during the aging process. Throughout aging, tens to hundreds of nanometers of calcite either dissolve or precipitate, depending on the degree of saturation of the brine. However, this surface transformation process is primarily limited to regions of the substrate that are directly exposed to aging brine. Regions that are covered by a sessile oil drop are protected from both etching by an undersaturated brine and overgrowth by a supersaturated brine. We thus conclude that the bottoms of the holes and tops of the mesas represent the original calcite surface levels, whereas the ambient surface is either massively etched or overgrown depending on the brine composition. This interpretation is consistent with the fact that the microscopic morphology under the oil footprint resembles the original freshly cleaved calcite surface much more than does the surrounding region.

It is worth noting that the degree of dissolution and precipitation only becomes visible thanks to the protective effect of the oil droplets during aging. Earlier measurements of variations in the morphology and composition of calcite surfaces upon aging revealed substantial transformations. Raman spectroscopy and energy-dispersive X-ray spectroscopy (EDX) also demonstrated that precipitates formed at calcite−brine interfaces consist primarily of calcite with a small amount of $MgCO_3$, as well as small amounts of (polyaromatic) organic material.[22,29] This is consistent with the works of Rao et al.,[22,28] where the formation (from CRO-equilibrated formation brine and from CRO), chemical composition, and stability of organo-ionic layers on calcite surfaces were characterized using multiple analytical techniques. The analysis of calcite-bound layers indicates the graphitic ordering of polyaromatic hydrocarbons formed via π-stacking, ionic, and hydrogen bonding interactions. The adsorbents also contain polar groups (aromatic carboxylic acid, diaryl ketone, aromatic amines or pyridyls, and alcohols) conjugated to the asphaltenes.

However, since these surface transformations were taking place homogeneously across the entire sample, no conclusions could be drawn regarding the thickness of the dissolved or precipitated layers. The values observed here reveal that the surface transformation is massive (Figures 3 and 4). In fact, the entire calcite−brine interface is completely refreshed either by dissolution or precipitation within 2 days of aging or less. The appearance of the small "bumps" along the step edges outside the drop footprint in Figure 3a is consistent with this scenario. Such features have been reported in earlier studies of calcite−brine interface.[74−76] They are commonly attributed to enhanced dissolution and subsequent reprecipitation rate of carbonate mineral at edge sites not too far from chemical equilibrium. Reprecipitation is often believed to occur via nucleation of Amorphous Calcium Carbonate (ACC) nanoparticles at the calcite surface via an interface-coupled dissolution-reprecipitation mechanism.[57,58] The details of the

https://doi.org/10.1021/acs.energyfuels.3c04467
Energy Fuels 2024, 38, 6723−6737

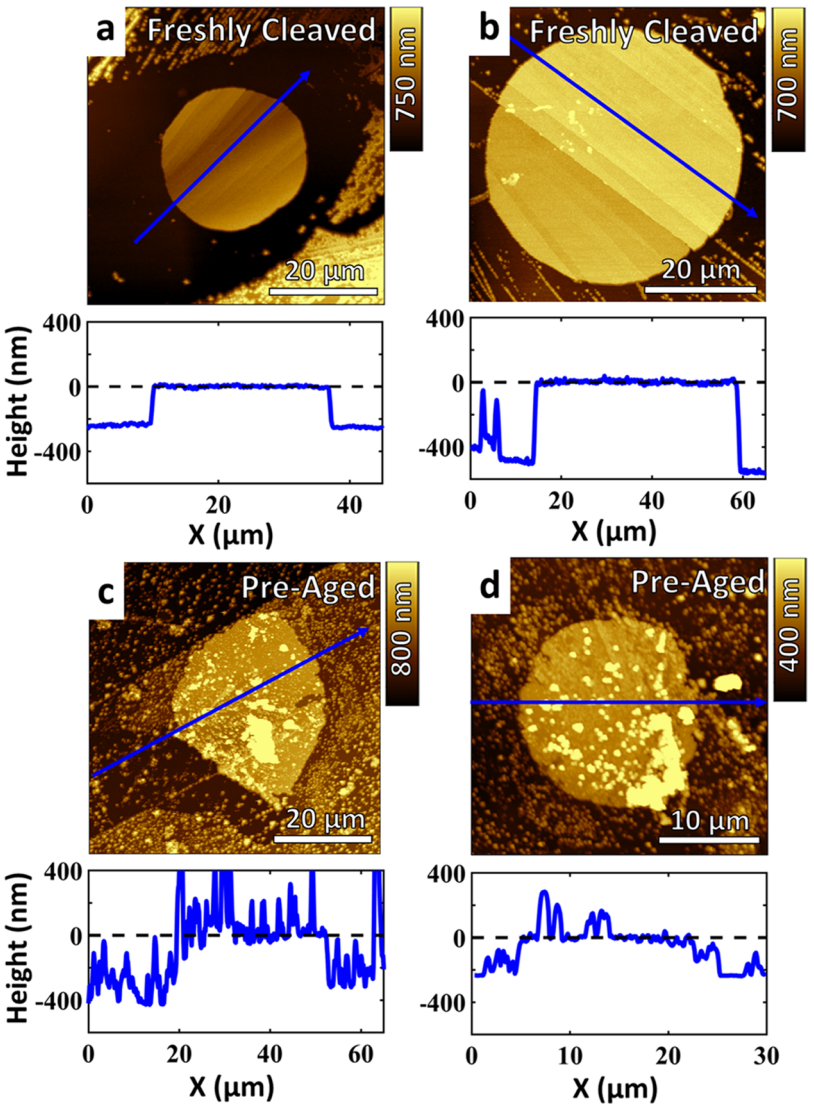

Figure 5. AFM topography scans of oil droplet locations on (a, b) freshly cleaved calcite or (c, d) preaged calcite after aging for 1 (d) to 2 weeks (a–c) at RT in 10× dil. HSW (a, c) and 4× [SO_4^{2-}] 10× dil. HSW (b, d). Shown height profiles correspond to the blue arrows in the topography scans.

process are most likely affected by the presence of organics dissolved in the nearby crude oil.

The same aging procedure was repeated for all brines listed in Table 1 at RT. Notwithstanding substantial heterogeneity and variations from sample-to-sample and drop-to-drop a clear correlation of dissolution vs precipitation with the saturation index of the brine could be established (Figure 4). The two higher-salinity brines, HSW and FW, both cause precipitation. Interestingly, the difference in precipitation between FW and HSW is rather weak, irrespective of the much higher degree of supersaturation of FW (Table 1). The precipitation, as measured from the AFM height profile next to the three-phase contact line, amounts to a few tens of nanometers and varies little after a few days. Conversely, all of the undersaturated low-salinity brines cause dissolution and mesa-like protrusions bound by the COBR pinned contact line. Their height increases over the time span of the experiment up to several hundreds of nanometers, with no indication of saturation even after 2 weeks of aging. Dissolution is thus more pronounced than precipitation for the undersaturated fluids. Overall, our results highlight the relevance of mineral dissolution in the context of both geosciences and reservoir engineering.

Assuming a roughly linear dissolution rate for the 2-week experiments and diluted brines, we extract an approximate dissolution rate of $\approx 10^{-12}$ mol·cm^{-2}·s^{-1}. This value is somewhat different compared to what is reported in the literature.[77,78] However, one should note that our estimated dissolution rate is taken at the three-phase contact line. This is a key part of our methodology and is of particular relevance to mineral dissolution in the context of oil recovery. As calcite dissolution rates are highly dependent on brine composition, pH, surface-to-volume ratio, temperature, pressure, and flow conditions, it is likely that local dissolution rates around the three-phase contact line are different from bulk dissolution rates, where the calcite is not in contact with oil. Furthermore, Smith et al., who used similar calcite substrates and similarly complex low-salinity brines, reported comparable constant dissolution rates as observed in Figure 4.[79] Interestingly, the observed dissolution rates hardly vary between 10× dil. HSW and its SO_4^{2-}-enriched variant. Similarly, preaging the calcite samples in equilibrated FW had little effect on the dissolution

https://doi.org/10.1021/acs.energyfuels.3c04467
Energy Fuels 2024, 38, 6723−6737

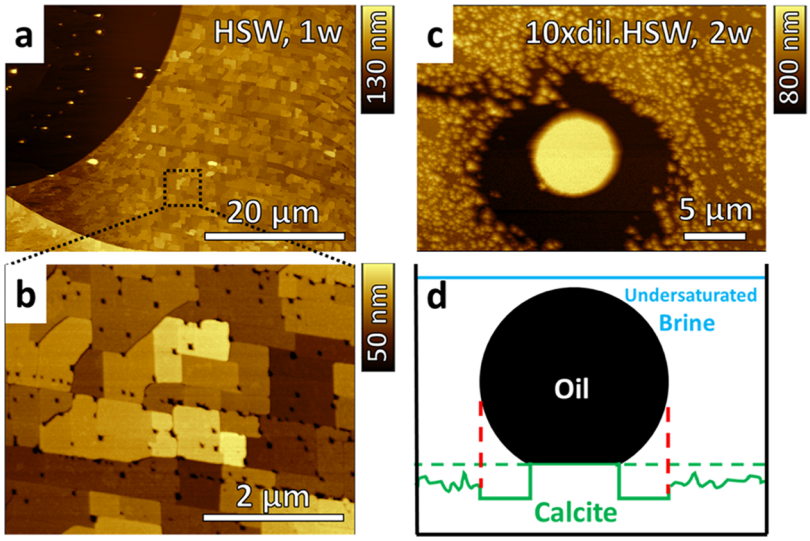

Figure 6. (a–c) AFM topography scans of oil droplet locations on calcite after aging at RT in (a, b) HSW for 1 week and (c) 10× dil. HSW for 1 week. Scan (b) was recorded in the area enclosed by the yellow square in (a). (d) Schematic of an experiment during aging, showing a possible explanation for the halo-like feature observed in (c).

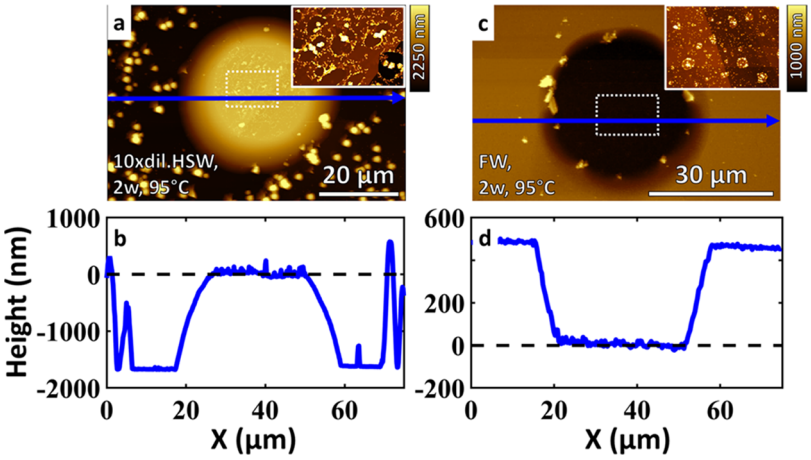

Figure 7. AFM topography scans of oil droplet locations on calcite after aging for 2 weeks at 95 °C in (a) 10× dil. HSW and (c) FW, with an inset showing corresponding detailed views of the oil–calcite contact areas. Height profiles corresponding to the blue arrows in (a) and (c) are shown in (b) and (d), respectively, at different scales.

rates within the experimental resolution. Only for the Mg^{2+}-enriched diluted brine, a statistically significant reduction in the dissolution rate is observed.

3.3. Microscopic Surface Properties. While preaging thus has little effect on the average height difference, it nevertheless strongly affects the microscopic structure of the surface (Figure 5). Preaged samples (Figure 5c,d) show a rougher topography than freshly cleaved ones (Figure 5a,b), both underneath and adjacent to the locations of the oil drops. The shape of the pinned contact line at the edge of the mesas also differs. For freshly cleaved samples, the contact line generally looks more smooth and circular than for preaged samples. Most likely, this reflects the presence and relevance of more pronounced pinning sites during the early stages of sample preparation (i.e., when the oil puddle breaks up into droplets, Figure 2b). Irrespective of preaging the substrate, the SO_4^{2-} enrichment of 10× dil. HSW (Figure 5b,d) does not appear to affect the topography and calcite dissolution rate at the three-phase contact line any differently than regular 10× dil. HSW (Figure 5a,c).

As noted above, the samples display a substantial degree of variability between the different droplets. Nevertheless, a few additional scenarios were observed recurrently in addition to the general trends described above. Figure 6a,b shows an example of a pattern that has been observed exclusively and repeatedly after aging in HSW. Rather than being smooth or displaying some random roughness, the precipitated layer seems to be broken up into patches with a characteristic width of several hundred nanometers. Each patch is rather flat on the top, but the average high level varies by tens of nanometers between adjacent patches. Boundaries are typically straight, and deep pits (black in Figure 6b) occur along boundaries, in particular at vertices where three or more patches meet. Straightness and orientation of the boundaries between adjacent patches suggest a correlation with the bulk crystal lattice. We suspect that this peculiar patchiness is related to accumulating elastic strains in the growing precipitate layer that eventually leads to fractures.[22,80−82] Another phenomenon that is frequently observed is the presence of a halo around the mesas after aging in undersaturated brines (Figure 6c,d). These

https://doi.org/10.1021/acs.energyfuels.3c04467
Energy Fuels 2024, 38, 6723−6737

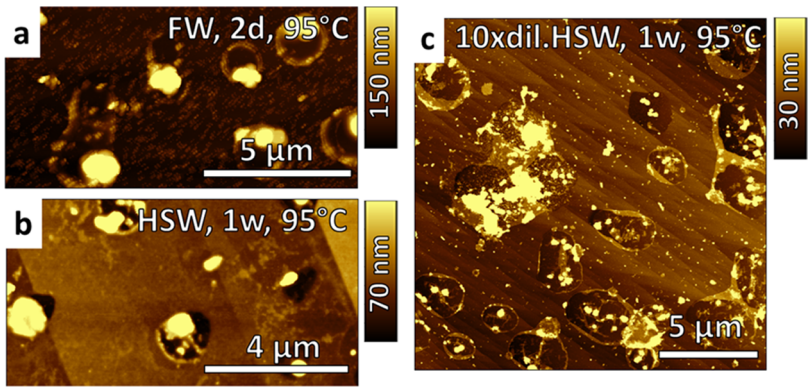

Figure 8. AFM topography scans of calcite areas protected by oil, imaged after aging at 95 °C in (a) FW for 2 days, (b) HSW for 1 week, and (c) 10× dil. HSW for 1 week. Small alterations to the calcite can be observed regardless of salinity, in the form of small circular or ellipsoidal islands. Characteristic calcite steps are often still visible alongside these small alterations.

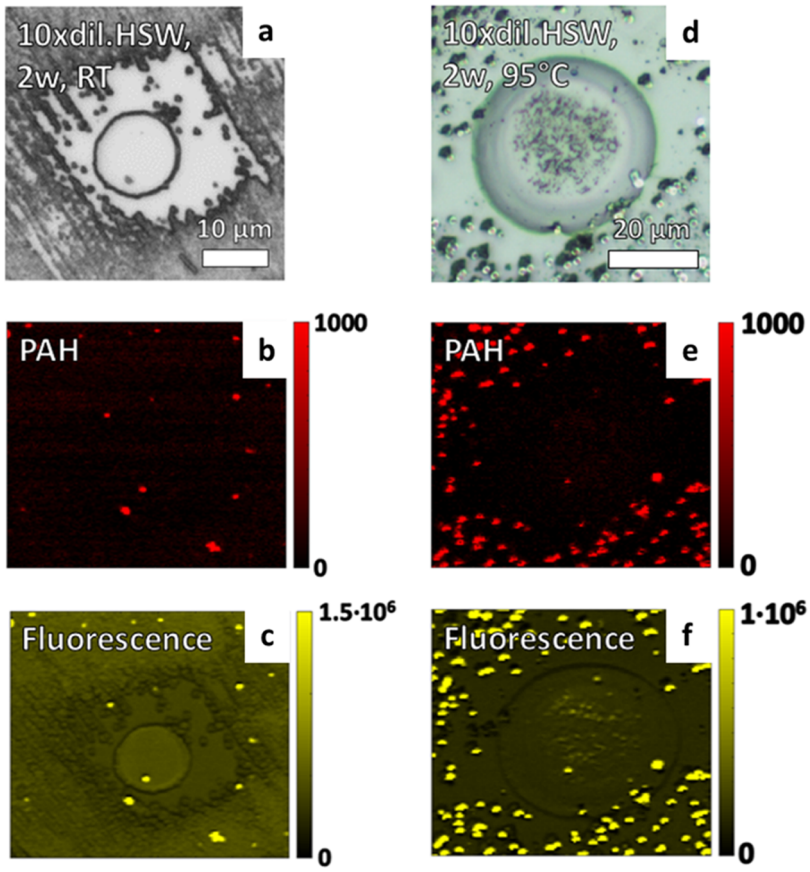

Figure 9. Bright-field microscopy (a, d) and CRM-derived x−y false color images showing distribution maps of polyaromatic hydrocarbons (PAH) (b, e) and fluorescence (c, f) around an oil droplet location after aging in 10× dil. HSW for 2 weeks at RT (a−c) and 95 °C (d−f).

halos are devoid of the otherwise omnipresent bumps of precipitated (organo-calcite) nanoparticles. The absence of nanoprecipitates suggests that the chemical composition of the brine in the vicinity of the three-phase contact line does not stimulate their formation and thus seems to be different from the bulk composition elsewhere at the solid−liquid interface. Such a different composition could arise due to the wedge-shaped confinement between CRO drop−brine interface and the substrate−brine interface as schematically illustrated in Figure 6d. Under nonequilibrium conditions that lead to precipitation, such a confinement geometry probably leads to transport limitations, inducing local variations of solute concentrations that may suppress precipitation.

Finally, we changed the aging temperature from RT to a reservoir-mimicking 95 °C. Examples using identical brines to Figure 3 for the undersaturated brine (10× dil. HSW with SI < 0) and supersaturated brine (FW with SI > 0) are given in Figure 7. Similar to RT (Figure 3), we observe mesas or holes at the original oil drop location for brines of low (Figure 7a) and high (Figure 7c) salinity, respectively. Nevertheless, there are a number of remarkable differences. First of all, the behavior between different drops displays a wider degree of variability. This is reflected in more pronounced variations in

https://doi.org/10.1021/acs.energyfuels.3c04467
Energy Fuels 2024, 38, 6723−6737

the average height and depth of the mesas and holes (Figure S4). Second, the edges of the mesas and holes tend to be less sharp than at RT. Instead, they display gradual slopes from the center plateau levels toward the surrounding substrate level, as illustrated by the cross sections in Figure 7b,d. We believe that this reflects less rigid pinning of the three-phase contact line. We rationalize the observations in Figure 7a,c in the following manner: originally, the drop-substrate interfacial area was approximately 40 μm wide, corresponding to the bottom of the mesa. As the calcite gradually dissolved during aging, dilute brine gradually accessed the calcite underneath the drop starting from the contact line, driven by the gradual desorption of the interfacial layer of polar oil components and the preferential wetting by brine. Apparently, this process is more pronounced at elevated temperatures as compared to RT, as inferred before from macroscopic experiments.[83]

Since it is generally well established that increasing the temperature decreases the oil contact angle,[38,83] the observation of a sloping edge could demonstrate a behavior in which a receding or advancing contact angle could affect the height changes observed around the three-phase contact line. In the case of dissolution, various bumps are once again observed next to the droplet. Compared to RT, the bumps are significantly bigger, frequently protruding even above the original level of the calcite, as indicated by the protected mesa. These bigger deposits are in line with expectations, as all brines become more saturated at 95 °C (Table 1). Comparing the step heights in Figure 7b,d to the RT results in Figure 3c,g, trends appear more exacerbated at 95 °C, signified by both more local precipitation in supersaturated FW as well as more local dissolution in undersaturated 10× dil. HSW. Although the former matches expectations, the latter does not match expectations based on bulk brine chemistry, as the solubility of calcite lowers at higher temperatures, as indicated by the less negative Saturation Index (Table 1). However, it is worth repeating that we are looking at a three-phase contact line in the presence of complex organics, so deviation from simple bulk chemistry based only on brine is hardly remarkable. Furthermore, the area next to the droplet is altered significantly at higher temperatures. Also looking at the insets in Figure 7a,c and comparing them to the parallel experiments at RT in Figure 3a,c, one can see that the oil−calcite contact area is clearly less inert at elevated temperatures. This is reflected in a higher degree of surface roughness. Similar alterations are observed regardless of brine salinity, as shown in the close-ups of the oil−calcite interface in Figure 8. One can still rule out significant global dissolution or precipitation of the entire area under the droplet, as the characteristic steps of calcite can still often be discerned, but they are now interspersed with typically circular or ellipsoidal islands, containing one or more asperities. These islands suggest a highly localized dissolution-reprecipitation process caused by the presence of small brine droplets breaking up the oil−calcite interface. Due to the limited volume of these droplets, dissolved ions cannot diffuse far away from the surface, leading to reprecipitation of material within the droplets. We believe the mobility of brine toward the oil−calcite interface could be either osmotically driven through a thin brine film, or by water moving through the oil phase as microdispersions encapsulated by surfactants from the oil.[84−86]

Finally, performing Raman analysis (Figure 9) shows yet another striking difference between aging at RT and aging at 95 °C. After aging at RT, no significant presence of organics originating from the oil is observed on the substrate, neither underneath nor adjacent to the droplet locations. This could be due to the limited access of the brine underneath the oil droplets, which results in lower adsorption (below the detection limit by Raman spectroscopy) and/or weaker interaction of organic molecules with the calcite surface, which can subsequently be easily washed away by toluene rinsing (see Section 2). This changes significantly when aging at 95 °C. While the area underneath the droplet locations still seems mostly free from organics, all of the amorphous deposits adjacent to the droplets are covered in polyaromatic hydrocarbons (PAH) that were originally present in the oil droplet. Samples aged at 95 °C show a large degree of heterogeneity, much greater than at RT. This is represented by a large variance in all observed step heights (Figure S4) across different brines of variable salinity. Due to the local nature of AFM measurements, one needs to keep in mind that local trends of dissolution or precipitation may not be representative for the entire sample. Nevertheless, the topographical features presented here were observed multiple times in different brines and only ever after aging at 95 °C, never after aging at RT.

4. DISCUSSION

Macroscopic analysis techniques are often used to paint a microscopic picture of the calcite−crude oil−brine system, leaving the importance of mineral dissolution toward oil detachment unclear. The complexity of such a system mandates the buildup of correlations and averaging procedures that provide shortcuts to sidestep the microscopic details, which often hinders advancements to understand pore scale mechanisms in reservoir engineering.[1,87,88] Microscopic visualization of calcite dissolution is often attempted in the geosciences context with respect to the bulk material in the absence of any organics.[89−96] Despite the significance of those studies to estimate dissolution rates at different ionic strengths, saturation indices, and specific ions, the results from such studies cannot derive a clear picture for the mobilization of oil upon recovery. While others have already visualized the effect of calcite's surface roughness on the wettability of crude oil droplets,[97] we provide in this work for the first time a visualization of local dissolution and precipitation at the three-phase contact line between crude oil, calcite, and brine. The relevance of dissolution and precipitation in these reservoir-like systems must not be understated, as our results show that in addition to any changes in surface roughness, the base level of the surface goes up or down by hundreds of nanometers over the course of up to 2 weeks of aging in various brines at temperatures of 22 and 95 °C.

Generally, our results show that the saturation index matches the observed trend of either dissolution (for undersaturated brines) or precipitation (for supersaturated brines), with qualitatively the observed rate of precipitation being significantly less than the rate of dissolution. Considering the precipitates consist of primarily $CaCO_3$ with some additional incorporated Mg^{2+},[29] the total availability of these ions in the brine likely limits the total precipitation in our system. Increasing the Mg^{2+} content in 10× dil. HSW 4-fold was found to have a significant effect on the dissolution rate of calcite after aging at RT. After 2 days the results are inconclusive due to large error bars, but as the duration of the experiment increases it can be observed that the degree of dissolution in the Mg^{2+}-enriched brine starts to lag behind that of regular 10× dil. HSW. Comparing the results to the

https://doi.org/10.1021/acs.energyfuels.3c04467
Energy Fuels 2024, 38, 6723−6737

saturation indices in Table 1 seems remarkable, as the Mg^{2+}-enriched brine is similarly undersaturated with respect to calcite as regular 10× dil. HSW. In the literature, the actual effects of Mg^{2+} on calcite dissolution are a topic of debate, with various proposed mechanisms affecting the overall dissolution. At a pH range of 8−9, Compton and Brown observed strong inhibition of both calcite dissolution and precipitation by the presence of Mg^{2+} ions, attributed to the competitive Langmurian absorption of both Mg^{2+} and Ca^{2+} ions at the calcite surface.[98] Using brines around pH 7, Ruiz-Agudo et al.[91] concluded that two competing mechanisms are at play at room temperature. Mg^{2+} inhibits lateral spreading of etch pits, slowing down dissolution, but also promotes the dissolution along the surface normal. The balance between these two depends on the overall Mg^{2+} content of the brine, with the effect promoting dissolution only becoming dominant at higher Mg^{2+} concentrations of above 50 mM. Considering that even in 4× [Mg^{2+}] 10× dil. HSW the Mg^{2+} concentration is only ∼35 mM (see Table 1), our systems are predominantly subject to the inhibiting effect. Conversely, increasing the SO_4^{2-} content in 10× dil. HSW 4-fold did not produce significant differences in dissolution rates or surface topography during our experiments. Ruiz-Agudo et al.[91] also reported that the presence of SO_4^{2-} could increase both the density of etch pits as well as their dissolution along the surface normal. There is additionally also a significant dependence on the Mg^{2+} content as SO_4^{2-} can enhance the absorption of Mg^{2+} ions on carbonates, and Brady et al. reported increased dolomite ($CaMg(CO_3)_2$) precipitation in the presence of sulfate species in solution.[99] Over a range of 1 mM to 1 M, Ruiz-Agudo et al. found that NaCl and Na_2SO_4 had mostly comparable etch pit densities, with a slight increase observed for Na_2SO_4. Changing the brine to $MgCl_2$ increased the etch pit densities across the entire concentration range. Finally, although the presence of $MgSO_4$ caused the most etch pit spreading of all four brines at concentrations above 100 mM, it also showed the lowest density below concentrations of 10 mM. The brines used in our experiments have a total concentration of SO_4^{2-} less than 2 mM even after 4-fold enrichment (Table 1) due to practical considerations, as the presence of SO_4^{2-} can cause scaling and corrosion of pipeline infrastructure.[100] This lower concentration could explain why no significant effects in the dissolution rate between regular and SO_4^{2-}-enriched brines are observed in our experiments, particularly when considering the large statistical errors arising from sample heterogeneity.

Preaging the calcite in eqFW has significant effects on the topography at the end of the experiments but not on the overall dissolution rate. A significant shift in topography and roughness is expected, as previous work has shown that the preaging procedure increases the rms roughness to 5.5 nm from the 2.5 nm of bare calcite.[42] Notably, this roughness increase occurs prior to the attachment of the oil droplets in the current experiments, which could explain why both the surface underneath and adjacent to the droplet appear more rough. Additionally, this explains why the pinned contact lines look less smooth. Since the reconstructed surface after the preaging step still consists primarily of calcite, it is no surprise that the dissolution rates are similar to those observed for freshly cleaved calcite.

After aging at 95 °C, the step heights at the three-phase contact line are too variable to clearly show any increased influence of the potential determining ions SO_4^{2-} and Mg^{2+} (Figure S4), despite the incorporation of Mg^{2+} into the calcite lattice as well as the calcite growth rate being known to increase with temperature.[101] However, there were various other observations that were made after aging at 95 °C and never when aging at 22 °C. We observe gradually sloping contact lines that could indicate that the contact line recedes or advances. Although droplets still neither detached nor moved significantly during aging, the edges of the oil droplets often become slightly distorted (Figure S5), further supporting the possibility of local mobility of the contact line. The circular or ellipsoidal islands often observed underneath the droplet at 95 °C do not depend significantly on organics from the oil, as they do not show up clearly during Raman analysis despite the ubiquitous presence of oil surrounding the small brine droplets that cause the formation of these islands. The mobility of the brine through the oil phase via microdispersions remains plausible; however, they are expected to form exclusively in the presence of low-salinity brines.[84,86] This contrasts with our observations presented here, as the formation of these islands is generally independent of salinity and instead heavily depends on the temperature. Furthermore, we observe both wider and large bumps next to the droplet at 95 °C than at RT. With the Raman analysis showing these deposits to be covered in PAH, it seems likely that these organic macromolecules from the oil are stabilizing amorphous calcium carbonate (ACC) as it is formed via an interface-coupled dissolution-reprecipitation mechanism.[58] This effect being more pronounced at higher temperatures is expected, as the organics from the oil transfer into the brine phase more efficiently at these temperatures.[28,29,42,69] The seemingly contradictory observation of more dissolution at 95 °C than at RT is likely related as the excess dissolved calcite is stabilized in its intermediate amorphous form without further reprecipitating back into a crystalline layer. Raman analysis also detects the presence of PAH when analyzing preaged samples (Figure S6), even at RT. However, there are no clear connections between the location of the oil droplets, and the locations of the PAH. This PAH has therefore likely been deposited from the equilibrated brine during the preaging procedure when the oil droplets were not yet present, as previous experiments have also shown the presence of PAH after the preaging procedure at 95 °C.[28]

Looking back at the complex three-phase system shown in Figure 1a−c, we can now identify several elements that correspond to the previously proposed processes. In diluted brines, the calcite exposed to the brine dissolves over time, whereas the calcite exposed to oil remains mostly inert. Dissolved ions may reprecipitate via amorphous phases as part of an interface-coupled dissolution-reprecipitation mechanism. Additionally, at elevated temperatures, an even more localized dissolution-reprecipitation process is occurring in small water droplets trapped under the oil. The source of the water droplets may be found in microdispersions of water in the oil phase, or osmotic swelling via a thin water film between the oil and calcite substrate. Furthermore, elevated temperatures lead to increased transfer of PAH organics from the oil into the brine. These organics find their way to the reactive calcite−brine interface where they alter the dissolution-reprecipitation equilibria.

5. CONCLUSIONS

Our work presents a method for the local visualization of dissolution and precipitation on model calcite surfaces in the presence of crude oil and ambient brine. The method leaves

https://doi.org/10.1021/acs.energyfuels.3c04467
Energy Fuels 2024, 38, 6723−6737

the three-phase contact line of oil droplets pinned, with the oil protecting the calcite underneath from alteration, while the ambient brine dissolves or precipitates the surrounding calcite. This protection effect was unaffected by roughening of the surface due to preaging the substrate in equilibrated reservoir brine (eqFW). The protected surface area provides an internal height reference, allowing for the determination of the degree of dissolution and precipitation in a particular brine. The effect of several brines with different salinity indices as well as ionic composition was first explored at room temperature (22 °C). Observations match expectations, with dissolution observed for undersaturated brines and precipitation observed for supersaturated brines. Moreover, the addition of SO_4^{2-} had little to no effect on mineral dissolution, whereas increasing the Mg^{2+} content slightly inhibited it. At elevated temperatures of 95 °C, the general protection mechanism persists while the system becomes more dynamic, with the magnitude of dissolution and precipitation increasing. Furthermore, organics moving from the oil phase into the brine phase are proposed to stabilize amorphous deposits on the altered substrate. The developed method is exploited in this work to improve our understanding of the relevance of mineral dissolution during low-salinity water flooding in carbonate reservoirs. More generally however, the method is easily adaptable to different temperatures, brine compositions, and potentially miscible CO_2, chemicals, polymers, as well as natural rock samples. Coupled with Raman and other advanced chemical analysis techniques, the methods can unlock doors to improving our understanding of subsurface phenomena in a representative setup at the microscopic scale.

■ ASSOCIATED CONTENT

Supporting Information

The Supporting Information is available free of charge at https://pubs.acs.org/doi/10.1021/acs.energyfuels.3c04467.

Crude oil compositional analysis; optical microscopy images of oil droplets on the calcite surface during in situ aging in variable brines and temperatures; AFM topography scan of the boundary between the calcite area covered by *n*-decane and brine; height differences between droplet locations and their surroundings as extracted from AFM high profiles after oil droplet-covered calcite was aged at 95 °C in variable brines; and bright-field and confocal Raman microscopy images showing the distribution of polyaromatic hydrocarbons on the calcite (PDF)

■ AUTHOR INFORMATION

Corresponding Authors

Igor Siretanu − *Physics of Complex Fluids Group and MESA+ Institute, Faculty of Science and Technology, University of Twente, 7500 AE Enschede, The Netherlands;* orcid.org/0000-0002-5741-9561; Email: i.siretanu@utwente.nl

Frieder Mugele − *Physics of Complex Fluids Group and MESA+ Institute, Faculty of Science and Technology, University of Twente, 7500 AE Enschede, The Netherlands;* orcid.org/0000-0003-3824-3617; Email: f.mugele@utwente.nl

Authors

Frank Megens − *Physics of Complex Fluids Group and MESA + Institute, Faculty of Science and Technology, University of Twente, 7500 AE Enschede, The Netherlands;* orcid.org/0009-0007-9840-2030

Amani O. Alghamdi − *The Exploration and Petroleum Engineering Center − Advanced Research Center (EXPEC ARC), Saudi Aramco, Dhahran 34465, Saudi Arabia*

Amy Z. Stetten − *Physics of Complex Fluids Group and MESA+ Institute, Faculty of Science and Technology, University of Twente, 7500 AE Enschede, The Netherlands*

Mohammed B. Alotaibi − *The Exploration and Petroleum Engineering Center − Advanced Research Center (EXPEC ARC), Saudi Aramco, Dhahran 34465, Saudi Arabia*

Subhash C. Ayirala − *The Exploration and Petroleum Engineering Center − Advanced Research Center (EXPEC ARC), Saudi Aramco, Dhahran 34465, Saudi Arabia*

Ali A. Yousef − *The Exploration and Petroleum Engineering Center − Advanced Research Center (EXPEC ARC), Saudi Aramco, Dhahran 34465, Saudi Arabia*

Complete contact information is available at: https://pubs.acs.org/10.1021/acs.energyfuels.3c04467

Author Contributions

F. Megens, I.S., and F. Mugele conceived and designed the experiments; F. Megens and A.O.A. carried out the experiments; Data analysis, F. Megens, A.O.A., and I.S.; Funding acquisition and project administration, F. Mugele; Supervision, I.S., A.Z.S., and F. Mugele; F. Megens, A.O.A., A.Z.S., I.S., and F. Mugele contributed to overall interpretation of data and their implications. Writing—review and editing, F. Megens, A.O.A., A.Z.S., S.C.A., M.B.A., A.A.Y., I.S., and F. Mugele. All authors have read and agreed to the published version of the manuscript.

Notes

The authors declare no competing financial interest.

■ ACKNOWLEDGMENTS

The authors thank Michel Duits for insightful discussions. F. Megens, I.S., and F. Mugele thank University of Twente and the Saudi Arabian Oil Company (Saudi Aramco) for the funding under Contract No. 6600041100.

■ REFERENCES

(1) Bartels, W.-B.; Mahani, H.; Berg, S.; Hassanizadeh, S. Literature review of low salinity waterflooding from a length and time scale perspective. *Fuel* **2019**, *236*, 338−353.

(2) Mahani, H.; Keya, A.; Berg, S.; Bartels, W.; Nasralla, R.; Rossen, W. Insights into the Mechanism of Wettability Alteration by Low-Salinity Flooding (LSF) in Carbonates. *Energy Fuels* **2015**, *29* (3), 1352−1367.

(3) Derkani, M. H.; Fletcher, A. J.; Abdallah, W.; Sauerer, B.; Anderson, J.; Zhang, Z. J. Low salinity waterflooding in carbonate reservoirs: Review of interfacial mechanisms. *Colloids Interfaces* **2018**, *2* (2), 20.

(4) Buckley, J.; Morrow, N. In *Improved Oil Recovery by Low Salinity Waterflooding: A Mechanistic Review*, 11th International Symposium on Evaluation of Wettability and Its Effect on Oil Recovery, Calgary, 2010; pp 6−9.

(5) Tetteh, J. T.; Brady, P. V.; Ghahfarokhi, R. B. Review of low salinity waterflooding in carbonate rocks: mechanisms, investigation techniques, and future directions. *Adv. Colloid Interface Sci.* **2020**, *284*, No. 102253.

(6) Myint, P. C.; Firoozabadi, A. Thin liquid films in improved oil recovery from low-salinity brine. *Curr. Opin. Colloid Interface Sci.* **2015**, *20* (2), 105−114.

(7) Katende, A.; Sagala, F. A critical review of low salinity water flooding: Mechanism, laboratory and field application. *J. Mol. Liq.* **2019**, *278*, 627−649.
(8) Sorbie, K.; Collins, I. In *A Proposed Pore-Scale Mechanism for How Low Salinity Waterflooding Works*, SPE Improved Oil Recovery Symposium, Tulsa, OK, 2010; pp 760−777.
(9) Hao, J.; Mohammadkhani, S.; Shahverdi, H.; Esfahany, M.; Shapiro, A. Mechanisms of smart waterflooding in carbonate oil reservoirs - A review. *J. Pet. Sci. Eng.* **2019**, *179*, 276−291.
(10) Rücker, M.; Bartels, W.; Singh, K.; Brussee, N.; Coorn, A.; van der Linde, H.; Bonnin, A.; Ott, H.; Hassanizadeh, S.; Blunt, M.; et al. The Effect of Mixed Wettability on Pore-Scale Flow Regimes Based on a Flooding Experiment in Ketton Limestone. *Geophys. Res. Lett.* **2019**, *46* (6), 3225−3234.
(11) Ricci, M.; Spijker, P.; Stellacci, F.; Molinari, J.; Voitchovsky, K. Direct Visualization of Single Ions in the Stern Layer of Calcite. *Langmuir* **2013**, *29* (7), 2207−2216.
(12) Herruzo, E. T.; Asakawa, H.; Fukuma, T.; Garcia, R. Three-dimensional quantitative force maps in liquid with 10 piconewton, angstrom and sub-minute resolutions. *Nanoscale* **2013**, *5* (7), 2678−2685.
(13) Siretanu, I.; Ebeling, D.; Andersson, M.; Stipp, S.; Philipse, A.; Stuart, M.; Van Den Ende, D.; Mugele, F. Direct observation of ionic structure at solid-liquid interfaces: a deep look into the Stern Layer. *Sci. Rep.* **2014**, *4*, No. 4956.
(14) Tracey, J.; Miyazawa, K.; Spijker, P.; Miyata, K.; Reischl, B.; Canova, F. F.; Rohl, A. L.; Fukuma, T.; Foster, A. S. Understanding 2D atomic resolution imaging of the calcite surface in water by frequency modulation atomic force microscopy. *Nanotechnology* **2016**, *27* (41), No. 415709.
(15) Klaassen, A.; Liu, F.; Mugele, F.; Siretanu, I. Correlation between electrostatic and hydration forces on silica and gibbsite surfaces: An atomic force microscopy study. *Langmuir* **2022**, *38* (3), 914−926.
(16) Savulescu, G.; Rücker, M.; Scanziani, A.; Pini, R.; Georgiadis, A.; Luckham, P. Atomic force microscopy for the characterisation of pinning effects of seawater micro-droplets in n-decane on a calcite surface. *J. Colloid Interface Sci.* **2021**, *592*, 397−404.
(17) Karoussi, O.; Skovbjerg, L.; Hassenkam, T.; Stipp, S.; Hamouda, A. AFM study of calcite surface exposed to stearic and heptanoic acids. *Colloids Surf., A* **2008**, *325* (3), 107−114.
(18) Ricci, M.; Segura, J.; Erickson, B.; Fantner, G.; Stellacci, F.; Voitchovsky, K. Growth and Dissolution of Calcite in the Presence of Adsorbed Stearic Acid. *Langmuir* **2015**, *31* (27), 7563−7571.
(19) Wojas, N. A.; Swerin, A.; Wallqvist, V.; Jarn, M.; Schoelkopf, J.; Gane, P.; Claesson, P. Surface-Modified and Unmodified Calcite: Effects of Water and Saturated Aqueous Octanoic Acid Droplets on Stability and Saturated Fatty Acid Layer Organization. *Langmuir* **2021**, *37* (48), 14135−14146.
(20) Gray, M. R.; Tykwinski, R. R.; Stryker, J. M.; Tan, X. Supramolecular assembly model for aggregation of petroleum asphaltenes. *Energy Fuels* **2011**, *25* (7), 3125−3134.
(21) Liu, J.; Zhao, Y.; Ren, S. Molecular dynamics simulation of self-aggregation of asphaltenes at an oil/water interface: formation and destruction of the asphaltene protective film. *Energy Fuels* **2015**, *29* (2), 1233−1242.
(22) Rao, A.; Schilderink, N.; Le-Anh, D.; Zeng, R.; Lievens, C.; Braunschweig, B.; Ayirala, S. C.; Alotaibi, M. B.; Duits, M. H.; Yousef, A.; Mugele, F. Formation and Stability of Heterogeneous Organo−Ionic Surface Layers on Geological Carbonates. *Energy Fuels* **2022**, *36* (14), 7414−7433.
(23) Rosales, I.; Pomar, L.; Al-Awwad, S. Microfacies, diagenesis and oil emplacement of the Upper Jurassic Arab-D carbonate reservoir in an oil field in central Saudi Arabia (Khurais Complex). *Mar. Pet. Geol.* **2018**, *96*, 551−576.
(24) Frye, G.; Thomas, M. Adsorption of organic compounds on carbonate minerals: 2. Extraction of carboxylic acids from recent and ancient carbonates. *Chem. Geol.* **1993**, *109* (1−4), 215−226.
(25) Mohammadi, M.; Mahani, H. Direct insights into the pore-scale mechanism of low-salinity waterflooding in carbonates using a novel calcite microfluidic chip. *Fuel* **2020**, *260*, No. 116374.
(26) Chen, S.-Y.; Kristiansen, K.; Seo, D.; Cadirov, N.; Dobbs, H.; Kaufman, Y.; Schrader, A.; Eguiluz, R.; Alotaibi, M.; Ayirala, S.; et al. Time-Dependent Physicochemical Changes of Carbonate Surfaces from SmartWater (Diluted Seawater) Flooding Processes for Improved Oil Recovery. *Langmuir* **2019**, *35* (1), 41−50.
(27) Chen, S.-Y.; Kaufman, Y.; Kristiansen, K.; Seo, D.; Schrader, A.; Alotaibi, M.; Dobbs, H.; Cadirov, N.; Boles, J.; Ayirala, S.; et al. Effects of salinity on oil recovery (the "Dilution Effect"): Experimental and theoretical studies of crude oil/brine/carbonate surface restructuring and associated physicochemical interactions. *Energy Fuels* **2017**, *31* (9), 8925−8941.
(28) Rao, A.; Kumar, S.; Annink, C.; Le-Anh, D.; Ayirala, S.; Alotaibi, M.; Siretanu, I.; Duits, M.; Yousef, A.; Mugele, F. Mineral Interfaces and Oil Recovery: A Microscopic View on Surface Reconstruction, Organic Modification, and Wettability Alteration of Carbonates. *Energy Fuels* **2020**, *34* (5), 5611−5622.
(29) Rao, A.; Kumar, S.; Annink, C.; Le-Anh, D.; Alotaibi, M.; Ayirala, S.; Siretanu, I.; Duits, M.; Mugele, F.; Yousef, A. In *Artificial Diagenesis of Carbonates: Temperature Dependent Inorganic and Organic Modifications in Reservoir Mimetic Fluids*, SPE Improved Oil Recovery Conference, 2020; pp 3222−3236.
(30) Rao, A.; Ayirala, S. C.; Alotaibi, M. B.; Duits, M. H.; Yousef, A.; Mugele, F. Nonmonotonic Coupled Dissolution-Precipitation Reactions at the Mineral-Water Interface (Adv. Funct. Mater. 51/2021). *Adv. Funct. Mater.* **2021**, *31* (51), No. 2170379.
(31) Ayirala, S. C.; Al-Yousef, A.; Li, Z.; Xu, Z. Water ion interactions at crude-oil/water interface and their implications for smart waterflooding in carbonates. *SPE J.* **2018**, *23* (05), 1817−1832.
(32) Perles, C.; Guersoni, V.; Bannwart, A. Rheological study of crude oil/water interface−The effect of temperature and brine on interfacial film. *J. Pet. Sci. Eng.* **2018**, *162*, 835−843.
(33) Chávez-Miyauchi, T. E.; Firoozabadi, A.; Fuller, G. Nonmonotonic elasticity of the crude oil−brine interface in relation to improved oil recovery. *Langmuir* **2016**, *32* (9), 2192−2198.
(34) Moradi, M.; Alvarado, V. Influence of aqueous-phase ionic strength and composition on the dynamics of water−crude oil interfacial film formation. *Energy Fuels* **2016**, *30* (11), 9170−9180.
(35) Bartels, W.-B.; Mahani, H.; Berg, S.; Menezes, R.; van der Hoeven, J. A.; Fadili, A. Oil configuration under high-salinity and low-salinity conditions at pore scale: a parametric investigation by use of a single-channel micromodel. *SPE J.* **2017**, *22* (05), 1362−1373.
(36) Freer, E. M.; Radke, C. Relaxation of asphaltenes at the toluene/water interface: diffusion exchange and surface rearrangement. *J. Adhes.* **2004**, *80* (6), 481−496.
(37) Pierre, A.; Lamarche, J.; Mercier, R.; Foissy, A.; Persello, J. Calcium as potential determining ion in aqueous calcite suspensions. *J. Dispersion Sci. Technol.* **1990**, *11* (6), 611−635.
(38) Zhang, P.; Austad, T. Wettability and oil recovery from carbonates: Effects of temperature and potential determining ions. *Colloids Surf., A* **2006**, *279* (1−3), 179−187.
(39) Zhang, P.; Tweheyo, M.; Austad, T. Wettability alteration and improved oil recovery by spontaneous imbibition of seawater into chalk: Impact of the potential determining ions Ca2+, Mg2+, and SO42−. *Colloids Surf., A* **2007**, *301* (1−3), 199−208.
(40) Freer, E.; Svitova, T.; Radke, C. The role of interfacial rheology in reservoir mixed wettability. *J. Pet. Sci. Eng.* **2003**, *39* (1−2), 137−158.
(41) Kaminsky, R.; Radke, C. Asphaltenes, water films, and wettability reversal. *SPE J.* **1997**, *2* (04), 485−493.
(42) Kumar, S.; Rao, A.; Alotaibi, M.; Ayirala, S.; Yousef, A.; Siretanu, I.; Mugele, F. Response of crude oil deposited organic layers to brines of different salinity: An atomic force microscopy study on carbonate surfaces. *Fuel* **2021**, *302*, No. 121129.
(43) Lyu, C.; Zhong, L.; Ning, Z.; Chen, M.; Cole, D. Review on Underlying Mechanisms of Low Salinity Waterflooding: Comparisons

https://doi.org/10.1021/acs.energyfuels.3c04467
Energy Fuels 2024, 38, 6723−6737

between Sandstone and Carbonate. *Energy Fuels* **2022**, *36* (5), 2407−2423.
(44) Deng, X.; Kamal, M.; Patil, S.; Hussain, S.; Zhou, X. A Review on Wettability Alteration in Carbonate Rocks: Wettability Modifiers. *Energy Fuels* **2020**, *34* (1), 31−54.
(45) Al-Shalabi, E. W.; Sepehrnoori, K. A comprehensive review of low salinity/engineered water injections and their applications in sandstone and carbonate rocks. *J. Pet. Sci. Eng.* **2016**, *139*, 137−161.
(46) Vledder, P.; Fonseca, J.; Wells, T.; Gonzalez, I.; Ligthelm, D. In *Low Salinity Water Flooding: Proof of Wettability Alteration on a Field Wide Scale*, SPE Improved Oil Recovery Symposium, 2010.
(47) Ding, H.; Rahman, S. Experimental and theoretical study of wettability alteration during low salinity water flooding-an state of the art review. *Colloids Surf., A* **2017**, *520*, 622−639.
(48) Sagbana, P. I.; Sarkodie, K.; Nkrumah, W. A. A critical review of carbonate reservoir wettability modification during low salinity waterflooding. *Petroleum* **2023**, *9* (3), 317−330.
(49) RezaeiDoust, A.; Puntervold, T.; Strand, S.; Austad, T. Smart water as wettability modifier in carbonate and sandstone: A discussion of similarities/differences in the chemical mechanisms. *Energy Fuels* **2009**, *23* (9), 4479−4485.
(50) Lager, A.; Webb, K. J.; Black, C.; Singleton, M.; Sorbie, K. S. Low salinity oil recovery-an experimental investigation. *Petrophysics* **2008**, *49* (01), No. e1.
(51) Strand, S.; Høgnesen, E.; Austad, T. Wettability alteration of carbonates—Effects of potential determining ions (Ca2+ and SO42−) and temperature. *Colloids Surf., A* **2006**, *275* (1−3), 1−10.
(52) Chandrasekhar, S.; Sharma, H.; Mohanty, K. Dependence of wettability on brine composition in high temperature carbonate rocks. *Fuel* **2018**, *225*, 573−587.
(53) Den Ouden, L.; Nasralla, R.; Guo, H.; Bruining, H.; Van Kruijsdijk, C. In *Calcite Dissolution Behaviour During Low Salinity Water Flooding in Carbonate Rock, IOR 2015 − 18th European Symposium on Improved Oil Recovery*, 2015.
(54) Hiorth, A.; Cathles, L.; Madland, M. The impact of pore water chemistry on carbonate surface charge and oil wettability. *Transp. Porous Media* **2010**, *85* (1), 1−21.
(55) Xu, M.; Hu, X.; Knauss, K.; Higgins, S. Dissolution kinetics of calcite at 50−70 C: an atomic force microscopic study under near-equilibrium conditions. *Geochim. Cosmochim. Acta* **2010**, *74* (15), 4285−4297.
(56) Bonto, M.; Nick, H.; Eftekhari, A. Thermodynamic analysis of the temperature effect on calcite surface reactions in aqueous environments. *Energy Fuels* **2021**, *35* (20), 16677−16692.
(57) De Yoreo, J. J.; Gilbert, P.; Sommerdijk, N.; Penn, R.; Whitelam, S.; Joester, D.; Zhang, H.; Rimer, J.; Navrotsky, A.; Banfield, J.; et al. Crystallization by particle attachment in synthetic, biogenic, and geologic environments. *Science* **2015**, *349* (6247), No. aaa6760.
(58) Rodriguez-Navarro, C.; Burgos Cara, A.; Elert, K.; Putnis, C.; Ruiz-Agudo, E. Direct nanoscale imaging reveals the growth of calcite crystals via amorphous nanoparticles. *Cryst. Growth Des.* **2016**, *16* (4), 1850−1860.
(59) Sethmann, I.; Putnis, A.; Grassmann, O.; Löbmann, P. Observation of nano-clustered calcite growth via a transient phase mediated by organic polyanions: A close match for biomineralization. *Am. Mineral.* **2005**, *90* (7), 1213−1217.
(60) Gal, A.; Weiner, S.; Addadi, L. A perspective on underlying crystal growth mechanisms in biomineralization: solution mediated growth versus nanosphere particle accretion. *CrystEngComm* **2015**, *17* (13), 2606−2615.
(61) Albéric, M.; Bertinetti, L.; Zou, Z.; Fratzl, P.; Habraken, W.; Politi, Y. The Crystallization of Amorphous Calcium Carbonate is Kinetically Governed by Ion Impurities and Water. *Adv. Sci.* **2018**, *5* (5), No. 1701000.
(62) Bentov, S.; Weil, S.; Glazer, L.; Sagi, A.; Berman, A. Stabilization of amorphous calcium carbonate by phosphate rich organic matrix proteins and by single phosphoamino acids. *J. Struct. Biol.* **2010**, *171* (2), 207−215.
(63) Loste, E.; Wilson, R.; Seshadri, R.; Meldrum, F. The role of magnesium in stabilising amorphous calcium carbonate and controlling calcite morphologies. *J. Cryst. Growth* **2003**, *254* (1−2), 206−218.
(64) Rao, A.; Drechsler, M.; Schiller, S.; Scheffner, M.; Gebauer, D.; Cölfen, H. Stabilization of Mineral Precursors by Intrinsically Disordered Proteins. *Adv. Funct. Mater.* **2018**, *28* (37), No. 1802063.
(65) Cusack, M.; Freer, A. Biomineralization: elemental and organic influence in carbonate systems. *Chem. Rev.* **2008**, *108* (11), 4433−4454.
(66) Mann, S. *Biomineralization: Principles and Concepts in Bioinorganic Materials Chemistry*; Oxford University Press, 2001.
(67) Morse, J. W.; Arvidson, R.; Lüttge, A. Calcium carbonate formation and dissolution. *Chem. Rev.* **2007**, *107* (2), 342−381.
(68) Hassenkam, T.; Johnsson, A.; Bechgaard, K.; Stipp, S. Tracking single coccolith dissolution with picogram resolution and implications for CO2 sequestration and ocean acidification. *Proc. Natl. Acad. Sci. U.S.A.* **2011**, *108* (21), 8571−8576.
(69) Rao, A.; Ayirala, S.; Alotaibi, M.; Duits, M.; Yousef, A.; Mugele, F. Nonmonotonic Coupled Dissolution-Precipitation Reactions at the Mineral−Water Interface. *Adv. Funct. Mater.* **2021**, *31* (51), No. 2106396, DOI: 10.1002/adfm.202106396.
(70) Gustafsson, J. *Visual MINTEQ 3.0 User Guide* Department of Land and Water Resources, KTH: Stockholm, Sweden; 2011.
(71) Le-Anh, D.; Rao, A.; Schlautmann, S.; Stetten, A. Z.; Ayirala, S. C.; Alotaibi, M. B.; Duits, M. H.; Gardeniers, H.; Yousef, A.; Mugele, F. Effects of fluid aging and reservoir temperature on waterflooding in 2.5 D glass micromodels. *Energy Fuels* **2022**, *36* (3), 1388−1401.
(72) Stetten, A. Z.; Kratz, F. S.; Schilderink, N.; Ayirala, S.; Duits, M. H.; Kierfeld, J.; Mugele, F. Elastometry of Complex Fluid Pendant Capsules. *Langmuir* **2023**, *39* (46), 16303−16314.
(73) Nečas, D.; Klapetek, P. Gwyddion: an open-source software for SPM data analysis. *Open Phys.* **2012**, *10* (1), 181−188.
(74) Putnis, C. V.; Wang, L.; Ruiz-Agudo, E.; Ruiz-Agudo, C.; Renard, F. Crystallization via Nonclassical Pathways: Nanoscale Imaging of Mineral Surfaces. In *Aggregation, Biomineralization, Imaging & Application*; ACS Publications, 2021; pp 1−35.
(75) Hövelmann, J.; Putnis, C. V.; Benning, L. G. Metal sequestration through coupled dissolution−precipitation at the brucite−water interface. *Minerals* **2018**, *8* (8), 346.
(76) Wang, L.; Putnis, C. V. Dissolution and precipitation dynamics at environmental mineral interfaces imaged by in situ atomic force microscopy. *Acc. Chem. Res.* **2020**, *53* (6), 1196−1205.
(77) Arvidson, R.; Ertan, I.; Amonette, J.; Lüttge, A. Variation in calcite dissolution rates: A fundamental problem? *Geochim. Cosmochim. Acta* **2003**, *67* (9), 1623−1634.
(78) Morse, J. W.; Arvidson, R. The dissolution kinetics of major sedimentary carbonate minerals. *Earth-Sci. Rev.* **2002**, *58* (1−2), 51−84.
(79) Smith, M. E.; Knauss, K. G.; Higgins, S. R. Effects of crystal orientation on the dissolution of calcite by chemical and microscopic analysis. *Chem. Geol.* **2013**, *360−361*, 10−21.
(80) Dufresne, E. R.; Corwin, E.; Greenblatt, N.; Ashmore, J.; Wang, D.; Dinsmore, A.; Cheng, J.; Xie, X.; Hutchinson, J.; Weitz, D. Flow and fracture in drying nanoparticle suspensions. *Phys. Rev. Lett.* **2003**, *91* (22), No. 224501.
(81) Dufresne, E. R.; Stark, D.; Greenblatt, N.; Cheng, J.; Hutchinson, J.; Mahadevan, L.; Weitz, D. Dynamics of fracture in drying suspensions. *Langmuir* **2006**, *22* (17), 7144−7147.
(82) Xu, Y.; German, G.; Mertz, A.; Dufresne, E. Imaging stress and strain in the fracture of drying colloidal films. *Soft Matter* **2013**, *9* (14), 3735−3740.
(83) Lu, Y.; Najafabadi, N.; Firoozabadi, A. Effect of temperature on wettability of oil/brine/rock systems. *Energy Fuels* **2017**, *31* (5), 4989−4995.
(84) Emadi, A.; Sohrabi, M. In *Visual Investigation of Oil Recovery by Low Salinity Water Injection: Formation of Water Micro-Dispersions and Wettability Alteration*, SPE Annual Technical Conference and Exhibition, 2013.

https://doi.org/10.1021/acs.energyfuels.3c04467
Energy Fuels 2024, 38, 6723−6737

(85) Mahzari, P.; Sohrabi, M. In *Crude Oil/Brine Interactions and Spontaneous Formation of Micro-Dispersions in Low Salinity Water Injection*, SPE Improved Oil Recovery Symposium, 2014.
(86) Mahzari, P.; Sohrabi, M.; Cooke, A.; Carnegie, A. Direct pore-scale visualization of interactions between different crude oils and low salinity brine. *J. Pet. Sci. Eng.* **2018**, *166*, 73−84.
(87) Afekare, D. A.; Radonjic, M. From mineral surfaces and coreflood experiments to reservoir implementations: Comprehensive review of low-salinity water flooding (LSWF). *Energy Fuels* **2017**, *31* (12), 13043−13062.
(88) Dang, C.; Nghiem, L.; Nguyen, N.; Chen, Z.; Nguyen, Q. Mechanistic modeling of low salinity water flooding. *J. Pet. Sci. Eng.* **2016**, *146*, 191−209.
(89) Hillner, P.; Manne, S.; Gratz, A.; Hansma, P. AFM images of dissolution and growth on a calcite crystal. *Ultramicroscopy* **1992**, *42*−*44*, 1387−1393.
(90) Harstad, A.; Stipp, S. Calcite dissolution: Effects of trace cations naturally present in Iceland spar calcites. *Geochim. Cosmochim. Acta* **2007**, *71* (1), 56−70.
(91) Ruiz-Agudo, E.; Putnis, C.; Jiménez-López, C.; Rodriguez-Navarro, C. An atomic force microscopy study of calcite dissolution in saline solutions: The role of magnesium ions. *Geochim. Cosmochim. Acta* **2009**, *73* (11), 3201−3217.
(92) Ruiz-Agudo, E.; Kowacz, M.; Putnis, C.; Putnis, A. The role of background electrolytes on the kinetics and mechanism of calcite dissolution. *Geochim. Cosmochim. Acta* **2010**, *74* (4), 1256−1267.
(93) Stipp, S.; Eggleston, C.; Nielsen, B. Calcite surface structure observed at microtopographic and molecular scales with atomic force microscopy (AFM). *Geochim. Cosmochim. Acta* **1994**, *58* (14), 3023−3033.
(94) Lea, A.; Amonette, J.; Baer, D.; Liang, Y.; Colton, N. Microscopic effects of carbonate, manganese, and strontium ions on calcite dissolution. *Geochim. Cosmochim. Acta* **2001**, *65* (3), 369−379.
(95) Dong, S.; Berelson, W.; Adkins, J.; Rollins, N.; Naviaux, J.; Pirbadian, S.; El-Naggar, M.; Teng, H. An atomic force microscopy study of calcite dissolution in seawater. *Geochim. Cosmochim. Acta* **2020**, *283*, 40−53.
(96) Arvidson, R. S.; Collier, M.; Davis, K.; Vinson, M.; Amonette, J.; Luttge, A. Magnesium inhibition of calcite dissolution kinetics. *Geochim. Cosmochim. Acta* **2006**, *70* (3), 583−594.
(97) Al Maskari, N. S.; Sari, A.; Saeedi, A.; Xie, Q. Influence of surface roughness on the contact angle due to calcite dissolution in an oil−brine−calcite system: a nanoscale analysis using atomic force microscopy and geochemical modeling. *Energy Fuels* **2019**, *33* (5), 4219−4224.
(98) Compton, R. G.; Brown, C. The inhibition of calcite dissolution/precipitation: Mg2+ cations. *J. Colloid Interface Sci.* **1994**, *165* (2), 445−449.
(99) Brady, P. V.; Krumhansl, J.; Papenguth, H. Surface complexation clues to dolomite growth. *Geochim. Cosmochim. Acta* **1996**, *60* (4), 727−731.
(100) AlAbbas, F. M.; Williamson, C.; Bhola, S.; Spear, J.; Olson, D.; Mishra, B.; Kakpovbia, A. Microbial corrosion in linepipe steel under the influence of a sulfate-reducing consortium isolated from an oil field. *J. Mater. Eng. Perform.* **2013**, *22* (11), 3517−3529.
(101) Lopez, O.; Zuddas, P.; Faivre, D. The influence of temperature and seawater composition on calcite crystal growth mechanisms and kinetics: Implications for Mg incorporation in calcite lattice. *Geochim. Cosmochim. Acta* **2009**, *73* (2), 337−347.

https://doi.org/10.1021/acs.energyfuels.3c04467
Energy Fuels 2024, 38, 6723−6737